

University of Dundee

Centrifuge modelling of the use of discretely-spaced energy pile row to reinforce unsaturated silt

Vitali, Davide; Leung, Anthony; Feng, Song; Knappett, Jonathan; Ma, Li

Published in:
Geotechnique

DOI:
[10.1680/jgeot.20.P.157](https://doi.org/10.1680/jgeot.20.P.157)

Publication date:
2022

Licence:
CC BY

Document Version
Peer reviewed version

[Link to publication in Discovery Research Portal](#)

Citation for published version (APA):

Vitali, D., Leung, A., Feng, S., Knappett, J., & Ma, L. (2022). Centrifuge modelling of the use of discretely-spaced energy pile row to reinforce unsaturated silt. *Geotechnique*, 72(7), 618-631.
<https://doi.org/10.1680/jgeot.20.P.157>

General rights

Copyright and moral rights for the publications made accessible in Discovery Research Portal are retained by the authors and/or other copyright owners and it is a condition of accessing publications that users recognise and abide by the legal requirements associated with these rights.

- Users may download and print one copy of any publication from Discovery Research Portal for the purpose of private study or research.
- You may not further distribute the material or use it for any profit-making activity or commercial gain.
- You may freely distribute the URL identifying the publication in the public portal.

Take down policy

If you believe that this document breaches copyright please contact us providing details, and we will remove access to the work immediately and investigate your claim.

Centrifuge modelling of the use of discretely-spaced energy pile row to reinforce unsaturated silt

¹Vitali, D., ²Leung, A. K.*, ³Feng, S. ⁴Knappett, J. A., and ⁵Li, M.

ABSTRACT:

Discretely-spaced reinforced concrete (RC) energy pile rows have been proposed to be installed at the mid-height of soil slopes. While the pile row can provide mechanical reinforcement to the slopes, the piles can potentially be used to (i) intercept solar energy from roadways for heat storage in the ground to mitigate extreme high carriageway temperatures and also (ii) to extract shallow geothermal energy for road surface de-icing. In this study, a series of centrifuge model tests were conducted to evaluate the shearing behaviour of unsaturated silt with and without reinforcement by conventional piles and energy piles. Three-dimensional **finite element** coupled vapour-water-heat transport analysis was also performed to further understand the effects of pile heating on the responses of temperature and pore water pressure of the soil. The measured and computed results revealed that the primary effect of pile heating was an increase in soil hydraulic conductivity due to the heat-induced reduction in water viscosity. The heated soil had enhanced water flow and hence developed higher suction. When subjected to translational slip, the silt reinforced by a row of closely-spaced RC energy piles exhibited a more ductile shearing response and a lower peak shear resistance, compared to that reinforced by conventional piles. The peak bending moments mobilised in the energy piles in the stable stratum were also smaller. At larger shear displacements, however, the shear resistance converged to a similar value, regardless of the suction and temperature. These suggest that the piles modified with additional energy transfer functionality can continue to act as reinforcement, potentially preventing soil from a sudden brittle failure, without attracting additional flexural stresses onto the piles.

KEYWORD: Centrifuge modelling; Energy piles; Unsaturated soils; Suction; Slope stabilisation

¹ Consultant, Whole Life Consultants Ltd, Dundee, UK

² Assistant Professor, Department of Civil and Environmental Engineering, Hong Kong University of Science and Technology, Hong Kong SAR

³ College of Civil Engineering, Fuzhou University, China

⁴ Professor, School of Science and Engineering, University of Dundee, UK

⁵ Research student, School of Resource and Safety Engineering, Central South University, China

* Corresponding author, Email: ceanthony@ust.hk

INTRODUCTION

Extreme winter rainfalls and snowfalls due to climate change in the European temperate regions have caused increasing numbers of failures and disruption to road/railway embankments, bringing significant socio-economic losses (Sassa & Canuti, 2009; Huges *et al.*, 2008). While slope stability can be improved by soil nailing and piling (amongst other methods), traffic disturbance associated with road icing in winter is mitigated using de-icing salt, which aims to inhibit the crystallisation of water into ice and increase the grip of tyres. However, excessive use of salt can create environmental problems such as flooding due to the potential blockage of drainage as well as soil and water contamination due to the leaching of chlorine ions, potential chloride attack of reinforced concrete of pavements, bridges and retaining structures along with practical problems associated with salt storage and logistics and the environmental impact of quarrying large amounts of salt. In summer, extreme high summer temperatures (e.g., 38.7 °C in UK, July 2019; which broke the all-time maximum recorded temperature held by the UK Met Office) can also heat up the asphalt of the road as high as 50 °C. Such high temperatures lead to bitumen softening and damage due to rutting of the wearing course. While gritters might be brought in to spread dust and sand for road surface stabilisation, other measures are needed to reduce the thermal load of the road surface for protecting the infrastructure and preventing traffic disturbance.

Discretely-spaced reinforced concrete (RC) pile rows have been a common engineering method for improving slope stability (e.g., Poulos, 1995; Kourkoulis *et al.*, 2012; Al-Defae & Knappett, 2014) through the mobilisation of pile flexural strength (Smethurst & Powrie, 2007) and soil arching between the piles (Kourkoulis *et al.*, 2010; Girout *et al.*, 2016). An innovative and sustainable proposal advanced by the authors is to modify RC piles used for this purpose to be RC energy piles (Fig. 1). Solar energy may be intercepted and stored in heat-carrier fluid in a pipeline buried in the road pavement. The heat harvested can be pumped to the piles and the ground for heat storage when the road surface temperature is high. This operation leads to pile heating relative to the cooler surrounding soil. Using the same system, shallow geothermal energy at the bottom part of the piles (where soil is relatively warmer) may be extracted by the piles for road surface de-icing in winter months. The near-surface soil is affected by the winter atmospheric condition, and the soil temperature here would normally be lower than that in the pile carrying heated fluid. Hence, pile heating would also take place at shallow depths (where a slip surface may form) during this winter operation.

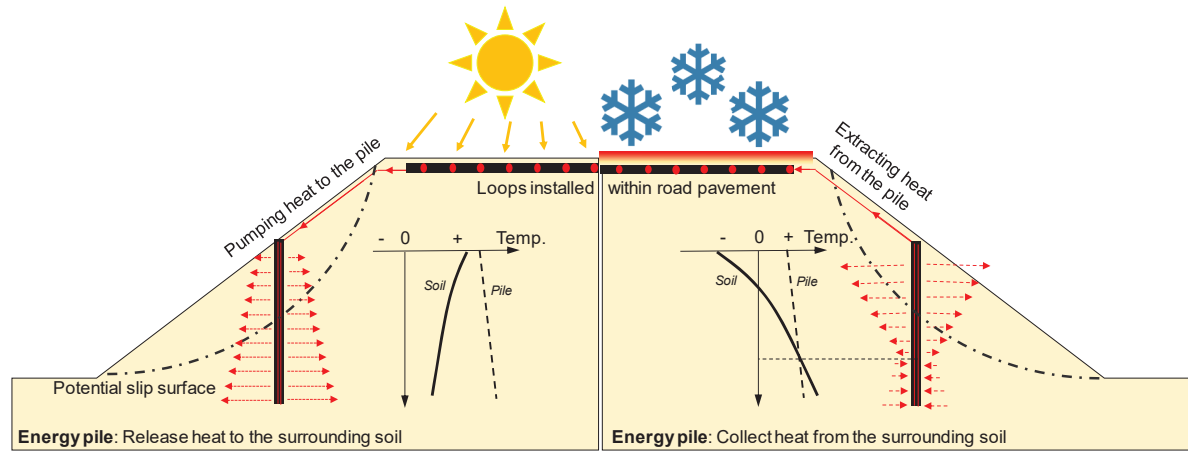


Figure 1. A schematic diagram showing the use of discrete energy pile row for slope stabilisation and road surface de-icing in “summer” and “winter” operation modes, respectively

Centrifuge modelling has been chosen as the principal research tool to study the fundamental mechanisms of the thermomechanical interaction between energy piles and unsaturated soil and hence to evaluate any effect of pile heating on the lateral behaviour of the soil-pile reinforcement system. By using a geotechnical centrifuge, testing a $1:N^{\text{th}}$ model at N times of the Earth’s gravity (g) through centripetal acceleration recreates stress levels that are close to much larger full-scale prototype systems (Taylor, 1995), correctly capturing the stress-dependent thermomechanical soil behaviour at homologous points. Indeed, there are physical model and centrifuge tests that have focused on the axial thermomechanical pile behaviour for building applications (Ng *et al.*, 2014; 2015; Goode & McCartney, 2015; Stewart & McCartney, 2014; Wu *et al.*, 2019). However, flexural thermomechanical pile behaviour, relevant to the system in Fig. 1, has never been studied before.

Correctly modelling the flexural behaviour of RC piles in a centrifuge is challenging as it requires careful selection of modelling materials to capture not only the nonlinear elasto-plastic-brittle behaviour (Knappett *et al.*, 2011), but also thermal properties such as thermal expansion coefficient of the energy pile (Vitali *et al.*, 2016). Additionally, effects of pile thermal loading on the changes in temperature and pore water pressure (PWP) fields in unsaturated soil (Leung *et al.*, 2020), and eventually the shear response of the energy pile-reinforced soil, are not well understood.

This paper aims to investigate and quantify the effects of pile heating on the flexural soil-energy pile interaction within soil translational slip and subsequently to understand the implications of energy pile use on the primary stabilisation function of the pile reinforcement. A series of

centrifuge model tests was carried out to measure any changes in the soil PWP due to pile heating and how these changes may have affected the lateral behaviour of an unsaturated soil reinforced by a row of discretely-spaced energy piles. To assist in the interpretation of the centrifuge test data, three-dimensional (3-D), **finite element**, water-vapour-heat transport back-analysis was additionally performed, with emphasis on the influences of pile heating on the soil water regime.

PROBLEM SIMPLIFICATION

The system of interest involves complex thermomechanical interaction between unsaturated soil and multiple energy piles in a sloping ground. Since the key objective of this study is to determine the thermo-hydro-mechanical behaviour of closely-spaced piles and the soil in their immediate vicinity for a given depth of soil slip, only a block of representative soil around piles, instead of an entire slope, was modelled in the centrifuge (Fig. 2). Following this simplification, the shear capacity of the soil-pile system can be determined by imposing a uniform translational displacement onto the back of the boundary of the “unstable” soil above a predefined horizontal slip. These simplifications are deemed realistic when: (i) the piles are sufficiently far from both the crest and toe of the slope; (ii) there exists a predefined slip; and (iii) the position of the slip is not modified by the presence of piles (Kourkoulis *et al.*, 2012). For condition (i), previous analyses (Poulos, 1995; Kourkoulis, 2009) have shown that uniform loading applied at distances greater than $5D$ (where D is pile diameter or width) away from the back of piles would introduce a reasonably uniform displacement profile across the unstable soil. When the three conditions are satisfied, the ultimate load acting on a row of stabilising pile would be a function of only the sliding depth, the pile configuration, and both the pile and soil properties.

The simplified block of a soil-pile system shown in Fig. 2 was tested in the centrifuge. Each pile has an aspect ratio (diameter : length) of 1:10. In total, three piles were considered within this block and they were socketed to a rigid bottom stratum for a length of $1D$. The piles were spaced, centre-to-centre, at $4D$, which is typical of field conditions (e.g., Smethurst & Powrie, 2007). The distance between the piles and the back of the model boundary was $6D$. The distance between the edge piles and the model boundary was $2D$ (i.e. half of the pile spacing), so the block can be tested under a plane strain condition, representing a repeating cell as part of a long piled slope.

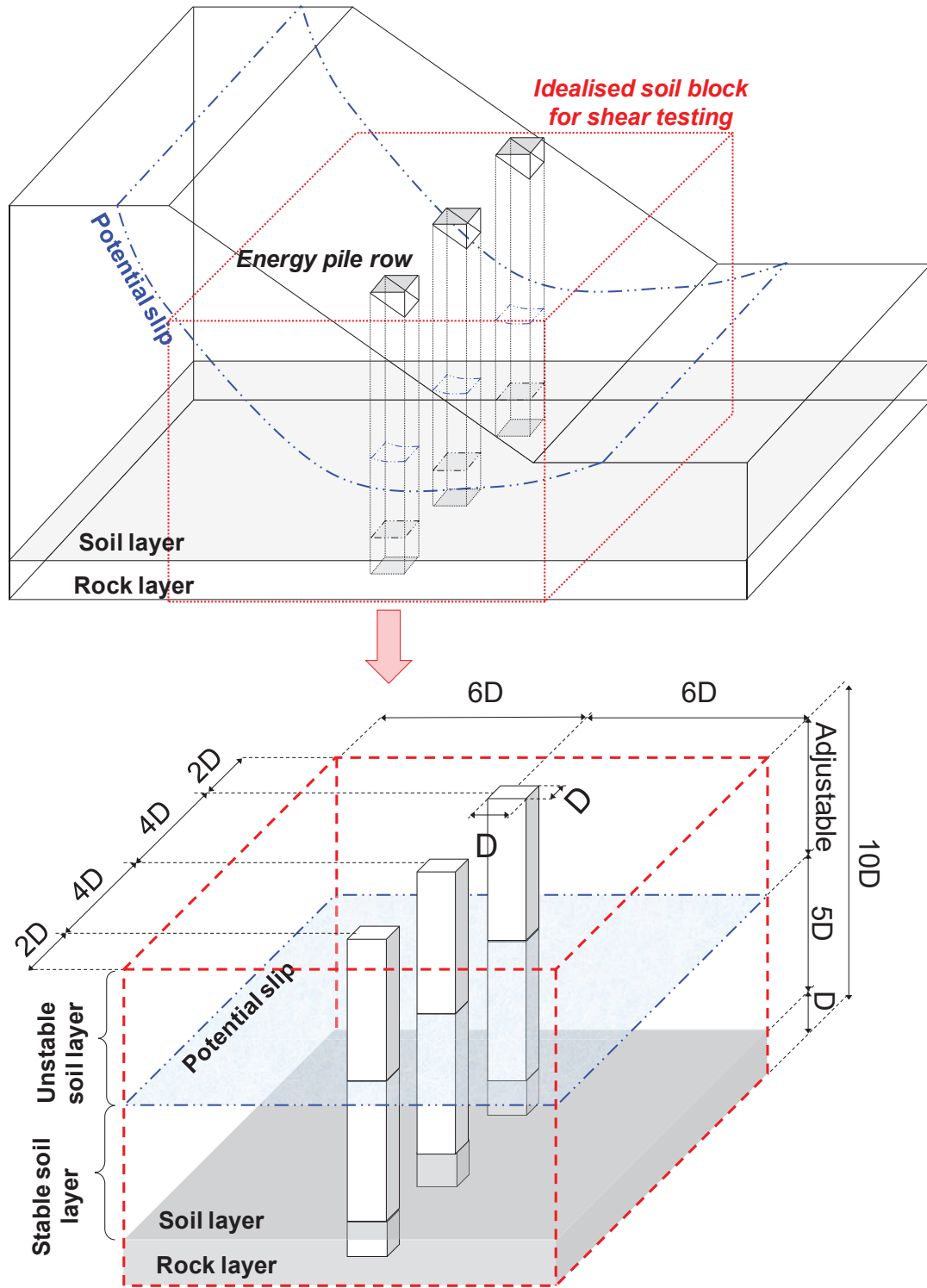


Figure 2. Model simplification for studying the shear behaviour of a block of soil reinforced by a discrete row of three reinforced concrete energy piles in the geotechnical centrifuge

CENTRIFUGE TEST PROGRAMME

Test plan

In total, four centrifuge tests were designed to evaluate the shear behaviour of a discrete energy pile row in unsaturated soil. All centrifuge tests were conducted using the 3.5 m radius Actidyn C67 geotechnical beam centrifuge at the University of Dundee, UK (Brennan *et al.*, 2014), all at 24 *g* ($N = 24$). Test 1 was a shearing-only test of an unsaturated silt without pile reinforcement. Test 2 was also a shearing-only test of the same soil type but reinforced by a discrete row of three conventional RC piles. Tests 3 and 4 were similar to Test 2, but reinforced by a row of three energy piles in each case and tested thermo-mechanically. Tests 3 and 4 represented the “operation” and “shutdown” modes of the system (further details below), respectively.

Test soil

The soil type tested was A50 silt with silica quartz content of more than 99.5%. The silt had a specific gravity of 2.65, and the particle diameters for 10%, 50% and 90% passing (i.e., d_{10} , d_{50} and d_{90}) were 0.004, 0.04 and 0.1 mm, respectively. Hence, the ratio between the thickness of a LDSA sample and d_{50} was 7500. This is well above 4700, beyond which the friction angle would be expected to become independent of sample size and almost the same as that obtained from drained torsional simple shear (Wu *et al.*, 2008). The drying and wetting water retention curves (WRC) of the silt, compacted to a dry density of 1.58 g/cm³ (equivalent to 95% degree of compaction; adopted in all the centrifuge tests) with an initial water content (by mass) of 18.5%, are shown in Fig. 3. The silt had an air-entry value of approximately 20 kPa, and it loses almost all the moisture as the matric suction reached 100 kPa. A noticeable hysteresis loop was observed after experiencing a cycle of drying and wetting. Based on constant-head permeability tests, the saturated hydraulic conductivity of the silt, determined at the same soil compaction level, was 8.3×10^{-7} m/s. Direct-shear tests on saturated and unsaturated silt over ranges of net normal stress (5 – 200 kPa) and suction (0 – 90 kPa) were conducted. The test data was interpreted by the Mohr-Coulomb failure envelop in the effective stress space:

$$\tau = c' + [(\sigma - u_a) + \chi(u_a - u_w)] \tan \phi' \quad (1)$$

where c' is cohesion; σ is total normal stress; u_a is pore air pressure (atmospheric); u_w is pore water pressure; ϕ' is friction angle; and χ is an effective stress parameter, which may be defined as

(s/s_e)^{0.55}, after Khalili & Khabbaz (1998), where s and s_e are the matric suction (i.e. ($u_a - u_w$)) and air-entry value, respectively. Based on the results shown in Fig. 4, the silt had a peak friction angle of 45.3°. The quartz-based silt, at dry condition, had a coefficient of thermal expansion of 0.55 $\mu\epsilon/^\circ\text{C}$ and a thermal conductivity (λ) of 6.5 W/(m K) (Cardarelli, 2008). Other silt properties are summarised in Table 1.

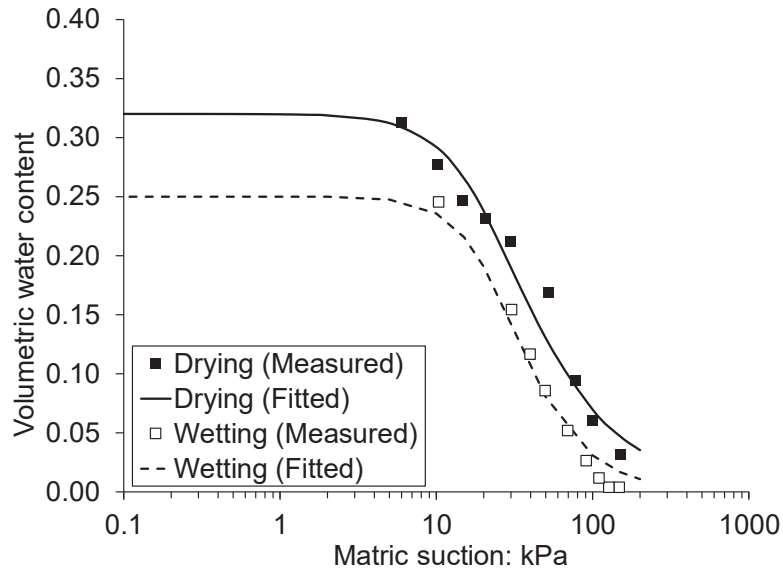


Figure 3. Drying and wetting WRCs of the silt, fitted with the van Genuchten (VG; 1980) equation. Fitting coefficients for the drying curve are $a = 0.00062 \text{ kPa}^{-1}$; $n = 1.09$; $m = 36.2$; $\theta_s = 0.32$ and $\theta_r = 0$, and those for the wetting curve are $a = 0.04 \text{ kPa}^{-1}$; $n = 2.5$; $m = 0.25$; $\theta_s = 0.25$ and $\theta_r = 0$.

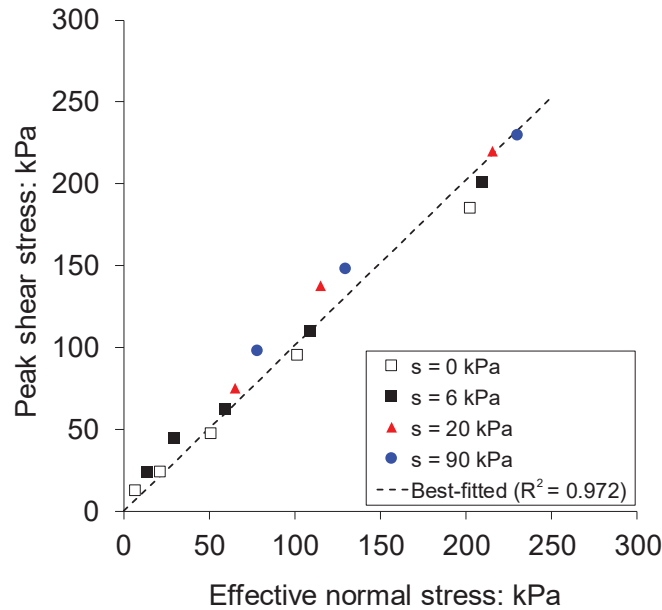


Figure 4. Effective stress failure envelope of the silt

Table 1. Properties of the silt used in the physical model tests

Parameter	Value
<i>Index properties</i>	
Specific gravity [-]	2.65
d_{10} (particle diameter with 10% passing) [mm]	0.004
d_{50} (particle diameter with 50% passing) [mm]	0.04
d_{90} (particle diameter with 90% passing) [mm]	0.1
Maximum dry density [kg/m^3]	1.66
Optimum water content [g/g]	0.191
<i>Mechanical properties</i>	
Peak friction angle [$^\circ$]	45.3
<i>Hydraulic properties</i>	
Air-entry value [kPa]	20
Saturated permeability [m/s]	8.3×10^{-7}
<i>Thermal properties</i>	
Thermal conductivity [W/(m K)]	6.5
Coefficient of thermal expansion [$\mu\epsilon/^\circ\text{C}$]	0.55

Model RC energy piles

The model piles used in this study were made of the model concrete developed by Vitali *et al.* (2016) and Zhao *et al.* (2020). This model concrete can realistically capture both the thermal and mechanical properties of concrete at prototype scale and also the nonlinear quasi-brittle behaviour that is highly important for correctly modelling the flexural behaviour of laterally-loaded reinforced concrete structures. The model concrete was a mixture of β -form surgical plaster, silica sand (Congleton HST95), water and copper powder (Phoenix Scientific Industries). While silica sand (particle diameter ranging from 0.06 to 0.3 mm, with $d_{50} = 0.2$ mm) is to geometrically scale down the size of aggregate in prototype concrete (Knappett *et al.*, 2011), the addition of copper powder (diameter ranging from 0.002 to 0.1 mm) aimed to enhance the thermal properties of the mortar. Element tests conducted by Vitali *et al.* (2016) and Zhao *et al.* (2020) showed that adding 6% copper powder (by volume) into the mix was able to reproduce the thermal conductivity (about 0.73 ± 0.09 W/(m K); mean \pm standard error of mean) of concrete, while not adversely affecting the mechanical properties of the mortar. Like concrete, the thermomechanical behaviour of the model concrete was subject to uncertainties due to material variabilities and workmanship. Statistical

analysis performed by Knappett *et al.* (2018) showed that the model concrete exhibited a similar coefficient of variation of mechanical strength ($< 10\%$) to full-scale concrete.

By using the model concrete, model piles were produced. A design moment capacity of 230 kNm was chosen to size the pile section, based on the test results of non-energy pile-reinforced slopes reported by Al-Defae & Knappett (2014) and Jeong *et al.* (2003). The pile design followed Eurocode 2 (EN 1992-1-1, 2004). In order to achieve the design moment, a doubly-reinforced 0.6 m x 0.6 m square pile with a length of 6 m and a steel reinforcement ratio of 2.1% was required (see section design in Fig. 5). Longitudinal reinforcement (bars) were applied both at the back and in the front of the pile section, with two 18 mm-diameter and four 14 mm-diameter mild steel bars on each side. Twenty-five transverse reinforcements (stirrups/shear links) of 14 mm diameter were also needed and they were spaced at 240 mm along the pile length.

For conducting the 24 *g*-centrifuge tests, the pile dimension was scaled down at 1:24. The model pile section is shown in Fig. 5. Stainless steel wire (Grade 316; Ormiston Wire Ltd) was used to produce the scaled longitudinal bars and shear links. While the longitudinal bars were produced by steel with a yield strength of 460 MPa and a model diameter of 1.25 mm (design requirement: 1.12 mm), the shear links were produced using steel with a yield strength of 380 MPa and a model diameter of 0.63 mm (design requirement: 0.59 mm). All the model longitudinal bars and shear links were coated with a thin layer of fine sand using epoxy for providing mechanical interlocking with the mortar (Knappett *et al.*, 2011).

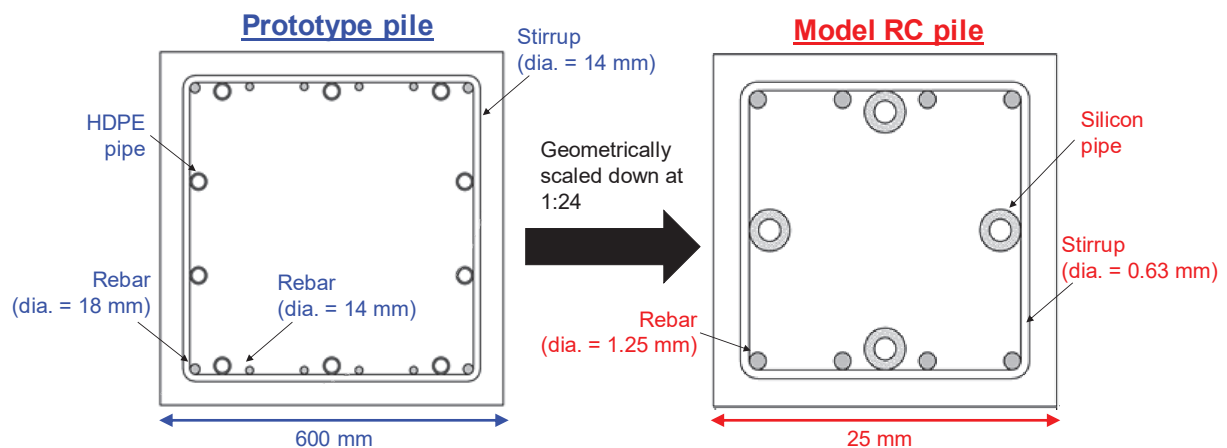
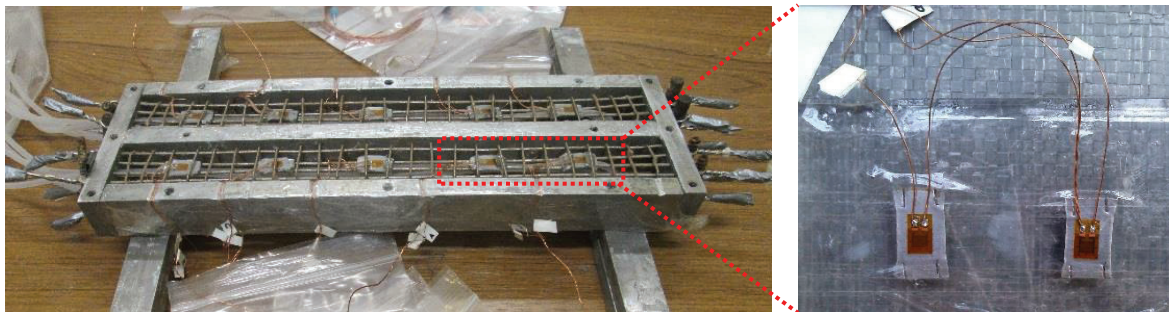


Figure 5. Structural design of pile cross section and its small-scale modelling for centrifuge testing. Note: the abbreviation “dia.” denotes diameter and HDPE stands for high-density polyethylene.

Two U-shaped tubes were used to circulate water of different temperature in and out of the pile using a centrifuge-mounted heat circulation system developed by Vitali *et al.* (2018). The pipe was made of flexible silicon, which was bent to form a U-shaped tube within the pile. The pipe had an internal diameter of 1.5 mm, a tensile strength of 10 MPa and the thermal expansion coefficient between 70 and 110 $\mu\epsilon/^\circ\text{C}$. The pipes were fixed onto the reinforcement cage (Fig. 6), which was assembled in an aluminium formwork, into which the model concrete was mixed with 6% copper powder (by volume) and then left to air-cure and harden for 28 days.



(a)



(b)



(c)

Figure 6. Model pile production: (a) positioning the steel reinforcement and U-shaped pipes; (b) strain-gauge installation on reinforcements; and (c) final product of the model RC pile after casting

Four-point bending tests were conducted to determine the flexural properties of the model piles. These showed that the 1:24 scale RC energy piles produced by the methods and procedures

above had representative prototype thermal expansion coefficient ($15.8 \mu\epsilon/^\circ\text{C}$), average peak moment capacity (336 kNm) and flexural rigidity (33 MNm^2), expressed at prototype scale (Minto *et al.*, 2016; Zhao *et al.*, 2020). The characteristic moment capacity of the pile as measured in the bending tests was higher than the design moment capacity, reflecting both the effects of the partial factors in the EC2 design procedure and the slight over-reinforcement due to the use of the slightly higher diameters of the model longitudinal bars with respect to the design values.

Test setup

Following the model simplification made to the soil-pile system (Fig. 2), a large-area ($300 \times 300 \times 300 \text{ mm}^3$) direct-shear apparatus (LDSA; Fig. 7) was developed to simulate the process of soil translational slip and to determine the shear resistance of the pile reinforcement in the centrifuge. The apparatus has two components. The first one is the shearing chamber, which is composed of four detachable aluminium square boxes stacked atop each other. These can be variously bolted together to create four potential shearing surfaces such that soil sliding at different depths can be modelled, with the upper-part moving. All the interfaces between the boxes are covered with polytetrafluoroethylene (PTFE) for minimising interface friction. The box interface has a frictional coefficient of 0.107. All horizontal force measurements presented in this study have been corrected for the box interface friction. Multiple ports are made on the sides of each box for installing thermocouples and high-capacity tensiometers to monitor changes in soil temperature and PWP during

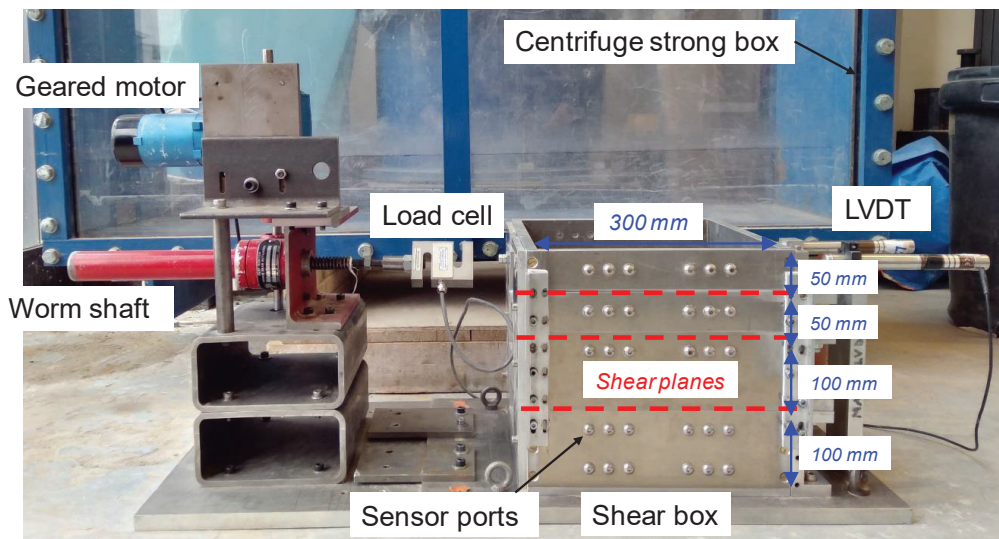


Figure 7. Overview of the large-area direct-shear apparatus (LDSA) for simulating and monitoring the process of soil translational slip in the geotechnical centrifuge

testing. The second component of the apparatus is the motor, which is used to drive a worm shaft to apply displacement-controlled horizontal loading to the back of the shearing chamber. A load cell is used to measure the shear loading mobilised, while a pair of linear variable differential transformers (LVDTs) are installed at the front face of the box for measuring the shear displacement (averaging the two measurements) and to check for any rotation about the vertical axis.

Figure 8 shows the overview and schematic diagram of the model setup of the centrifuge test. At the bottom of the LDSA, a 25 mm thick solid aluminium plate was placed with machined square slots to simulate the bedrock in the field and allow the piles to be socketed. Before soil compaction, three dummy piles with identical dimensions to the model RC piles but made of solid aluminium were socketed into the plate to a depth of $1D$. All the vertical surfaces of these piles were sleeved with polypropylene plastic sheets so that the post soil compaction extraction process would introduce minimal disturbance to the surrounding soil. The centre-to-centre spacing between these piles was $4D$. Installing the dummy piles at this stage aimed to prevent damage to the RC piles during soil compaction. Thereafter, soil thoroughly mixed to a uniform water content of 18.5% (by mass) was compacted into the LDSA by the moist tamping method. The soil compaction was divided into nine layers of equal height of 25 mm, targeting a uniform dry density profile of 1.58 g/cm^3 . The targeted dry density and water content (by mass) corresponded to an initial degree of saturation of the soil of 70%. After soil compaction, the dummy piles were extracted from the soil carefully and the model package was completed by socketing the three model RC piles into the bottom plate. This pile installation method may be representative to the case of cast-in-situ RC piles in practice.

Instrumentation

The central model pile and surrounding soil in each test was instrumented to monitor its thermo-mechanical behaviour during each centrifuge test. As shown in Fig. 8, three vertical arrays of four thermocouples at different depths were installed on the pile surface and also at $1D$ and $2D$ away from the pile surface within the soil, to monitor soil temperature changes induced by the model RC energy pile, both vertically and horizontally. Another array of five pairs of strain gauges (steel-foil; model no.: CAE-06-062UW-350; Micro-Measurements Ltd.) were installed to the same central model pile, four of which had approximately the same elevations as the thermocouples, for

monitoring mobilised bending moment during testing. The fifth pair of the strain gauges was installed in shallower pile depth of 25 mm (see the figure). Each strain gauge was affixed to a 0.3 mm-thick steel tab using a temperature resistant adhesive and the assembly was attached to two adjacent longitudinal bars (Fig. 6), mimicking the installation method adopted in full-scale RC piles in the field. Each pair of strain gauges was wired through half-bridge connections to allow bending moment measurement without parasitic axial loads or thermal effects. By mounting one gauge along the principal axis of strain (i.e., axial direction) and the other gauge in the same direction but on the opposite side of the model, temperature effects on the strain gauge responses can be eliminated (National Instruments, 2016).

In addition, a vertical array of three miniature high-capacity tensiometers (HCTs; model no. EPB-PW-7BS; StrainSense Ltd.) were installed to measure soil PWP change. Each HCT had a 3-bar ceramic stone, which can measure a range of PWP from -300 to 700 kPa. Prior to installation, each HCT was saturated following the rigorous procedures adopted by Zhou *et al.* (2006). Toll *et al.* (2013) have shown that temperature has minimal influence on the linear calibration factor (i.e., gradient of PWP and voltage; kPa/ μ V) of the HCTs.

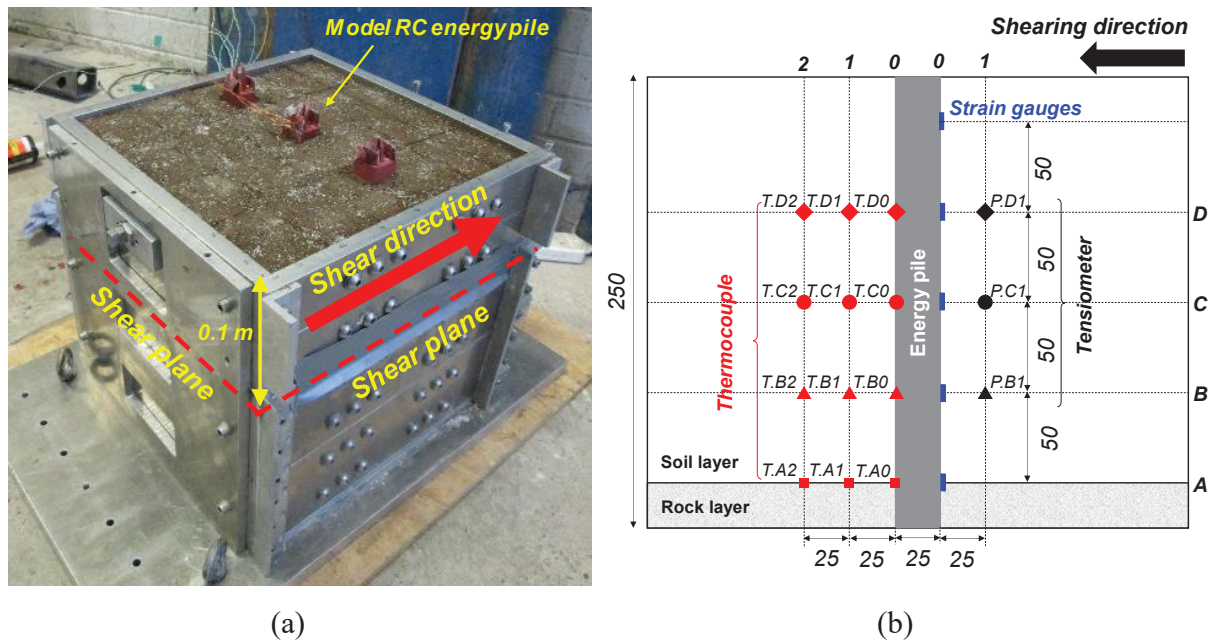


Figure 8. (a) Overview and (b) elevation view of the centrifuge model setup of the LDSA, together with the instrumentation plan (all dimensions are in mm)

Test procedures

The test procedures of all centrifuge tests broadly consisted of three consecutive steps, namely: (i) centrifuge spin-up; (ii) pile continuous heating; and (iii) direct shearing. In Step (i), the model package of each test was spun up to 24 *g*. Step (ii) only applied to Tests 3 and 4, where all three model RC energy piles were heated internally by maintaining an average inlet temperature (i.e., measured in the water immediately before entering the piles) at 42.5 °C for 90 – 120 days (prototype scale). This inlet temperature was typical of energy pile operation (e.g., Ng *et al.*, 2015; Stewart & McCartney, 2014). The adopted heating duration aimed to provide sufficient time to heat up the model RC pile so that the changes in pile surface temperature are representative of values normally recorded in the field (Liveridge & Powrie, 2013). Step (iii) applied to all four tests. In this step, constant-water-content shearing was carried out at 2.4 m depth (prototype), mimicking a translational slip. The shearing rate was controlled at 8.75×10^{-8} m/s (prototype), which is categorised as a “very slow” landslide (Dixon & Spriggs, 2007). Test 3 aimed to model soil failure during the “operation” mode of the system (refer to Fig. 1) upon heat storage in summer or heat extraction for road de-icing in winter. In both cases, the energy piles are expected to be hotter than the surrounding soil and actively heating; hence, in this test, the model piles were heated continuously during shearing. Test 4, on the contrary, modelled soil failure during the “shutdown” mode of the system under milder climate conditions, e.g. after a previous period of use but when heat is neither

Table 2. Scale factors (N = prototype model) relevant to this study (after Iai *et al.*, 2005)

Quantity	High-g scale factor
<i>General</i>	
Length	N
Stress	1
Pore water pressure or suction	1
Stiffness	1
<i>Structural-related</i>	
Bending stiffness	N^4
Lateral force	N^2
Lateral displacement	N
Bending moment	N^3
<i>Temperature-related</i> (Zhao <i>et al.</i> , 2020)	
Strain (thermal)	1
Time (diffusion)	N^2
Temperature change	1

harvested due to overcast weather in summer nor extracted in winter when the weather is warm enough to melt the road surface ice and not require active use of the system. From this point onwards, all quantities are expressed at prototype scale according to the scaling factors summarised in Table 2, unless stated otherwise.

FINITE ELEMENT BACK-ANALYSIS

To interpret the complex water-vapour-heat transport process involved in the heating of the unsaturated soil by the energy pile rows, three-dimensional (3-D) **finite element** (FE) simulations were carried out to back-analyse the responses of soil temperature and PWP during the 90-day pile heating. The governing equations presented by Leung *et al.* (2020) were adopted. To describe the water liquid and vapour transport, the **Richards equation (which is a combination of Darcy's law and continuity principle)** was used:

$$\frac{\partial \theta(T, \psi)}{\partial t} + \frac{\partial \theta_V(T, \psi)}{\partial t} = \nabla[(K_L(T, \psi) + K_V(T, \psi))(\frac{1}{\gamma_w} \nabla \psi + \nabla z) + (K_{LT}(T, \psi) + K_{VT}(T, \psi)) \nabla T] \quad (2)$$

where T is soil temperature; ψ is matric suction; $\theta(T, \psi)$ and $\theta_V(T, \psi)$ are volumetric liquid water content and volumetric water vapor content, respectively; $K_L(T, \psi)$ is the hydraulic conductivity of liquid water with respect to ψ change; $K_V(T, \psi)$ is the hydraulic conductivity of the water vapor with respect to ψ change; γ_w is unit weight of liquid water; $K_{LT}(T, \psi)$ is the hydraulic conductivity of liquid water with respect to T change; and $K_{VT}(T, \varphi)$ is the hydraulic conductivity of water vapor with respect to T change. On the other hand, the equations derived by Philip and de Vries (1957) were adopted to simulate heat transport:

$$C_s(\theta) \frac{\partial T}{\partial t} + L_0 \frac{\partial \theta_V}{\partial t} = \nabla[\lambda(\theta) \nabla T] - C_L q_L \nabla T - C_V \nabla(q_V T) - L_0 \nabla q_V \quad (3)$$

where $C_s(\theta)$, C_L and C_V are the volumetric heat capacities of soil, liquid water and water vapor, respectively; $\lambda(\theta)$ is a moisture-dependent thermal conductivity function (Chung & Horton, 1987); q_L and q_V are fluxes of liquid water and vapor, respectively; and L_0 is latent heat of vaporisation of liquid water. The coupling between Eqs (2) and (3) was made via the psychometric law:

$$H_r = \exp\left(\frac{\psi M}{\rho_w R T}\right) \quad (4)$$

where H_r is relative humidity; ρ_w is water density; M is molecular weight of water; and R is the universal gas constant (8.314 J/(K mol)). The mathematical formulation is similar to that reported

by Leung *et al.* (2020) but expressed in the 3-D condition for the problem of interest in this study. These equations were implemented into a **finite element** multi-physics platform, COMSOL v5.4. The soil hydraulic and thermal properties input to solve Eqs (2) – (4) are given in Table 3.

The geometry of the **finite element** mesh and the thermal and hydraulic boundary conditions were identical to what was tested at prototype scale (Fig. 9, following Fig. 2). At the soil surface, a constant ambient temperature of 23.1 °C and a relative humidity of 50% were specified and the evaporation rate was determined by the equation proposed by Wilson *et al.* (1997). Heat exchange across all sides was permitted by specifying the following equation:

$$Q_h = h(T - T_a) \quad (5)$$

where Q_h is the heat flux; T and T_a are the soil temperature and ambient temperature, respectively; and h is heat exchange coefficient, which was taken as 6.06 J/(m² s K) (Liu, 2017).

Table 3. Input parameters of soil's hydraulic and thermal properties

Parameters		Value
Water density [kg/m ³]		1000
Molecular weight of water [kg/mol]		0.018015
Universal gas constant [J/mol K]		8.314
VG parameters for fitting the drying water retention curve	Saturated volumetric water content [-]	0.32
	Residual volumetric water content [-]	0
	α [kPa ⁻¹]	0.00062
	n [-]	1.09
	m [-]	36.2
Hydraulic conductivity of saturated soil at 20 °C [m/s]		8.3×10^{-7}
Surface tension at 25 °C [kg/s ²]		0.07189
¹ Soil thermal conductivity	b_1 [-]	0.228
	b_2 [-]	-2.406
	b_3 [-]	4.909

¹the soil thermal conductivity was modelled as a function of soil volumetric water content (Chung & Horton, 1987) and the parameters are for silica soil taken from Chung & Horton (1987).

Test 3, which involved pile heating in the centrifuge test, was back-analysed. The simulation focused on the responses of soil temperature and PWP after reaching 24 *g* but before being subject to shearing. The initial soil temperature and PWP were specified based on the measurements made in the centrifuge test at 24 *g*. In this simulation, pile heating was modelled by specifying the distribution of pile surface temperature measured from the centrifuge test on the pile surface boundary.

Note that Test 4 (which also involved pile heating) was not separately modelled because the test condition and procedures before the shearing stage were identical to Test 3. To investigate the effects of pile heating on soil PWP changes, two additional simulations were conducted. One simulation considered pile heating but ignored vapour transport and water-vapour exchange, while the other ignored pile heating.

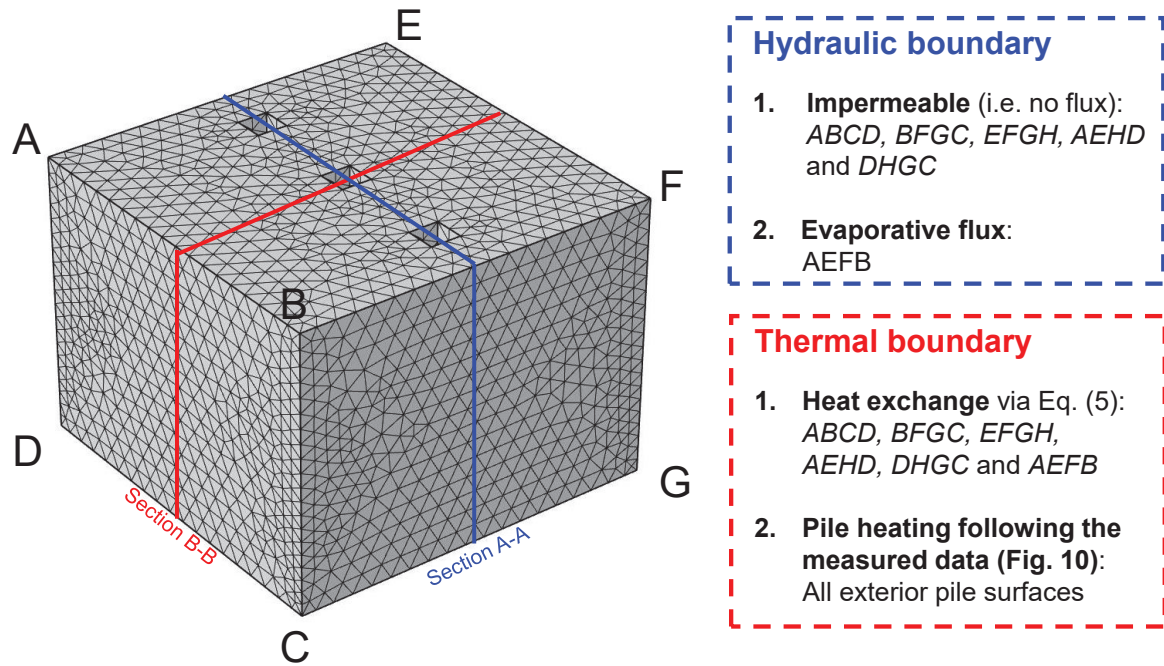


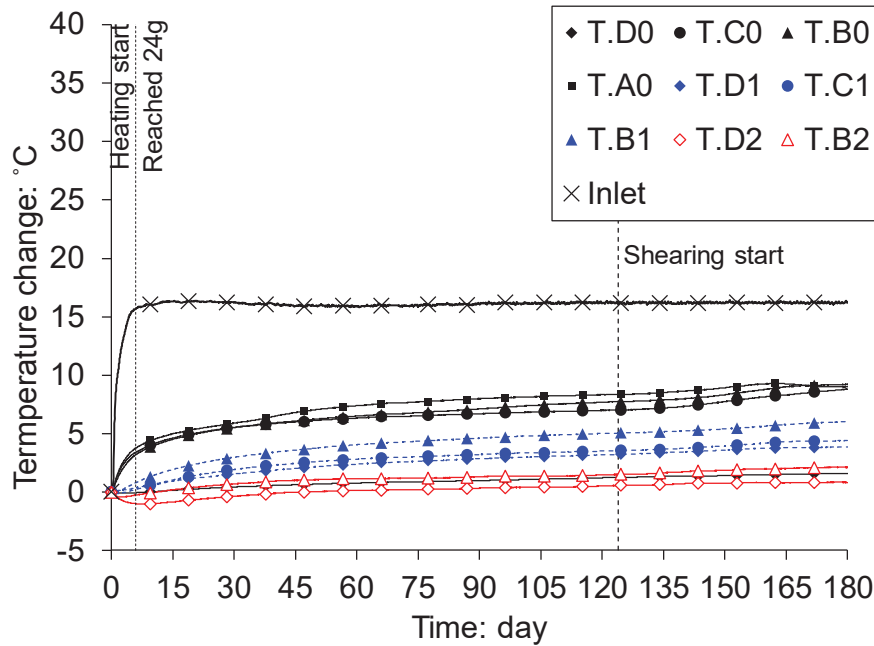
Figure 9. Finite element mesh and boundary conditions adopted in the numerical back-analysis.

RESULTS AND DISCUSSION

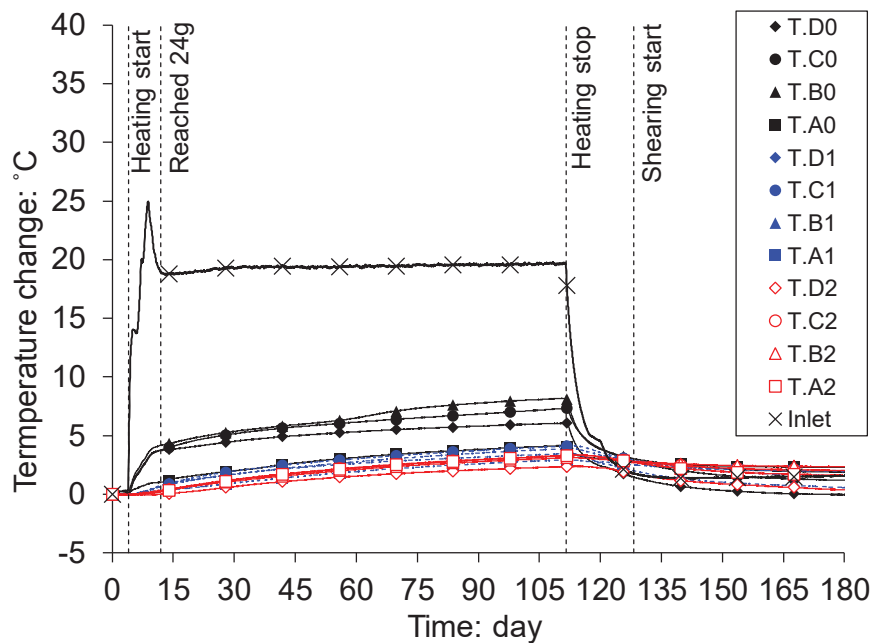
Heat transfer mechanisms and temperature field

Fig. 10 shows the measured variations of temperature change with time at different positions of the system in Tests 3 and 4. During heat transfer, some of the heat energy was absorbed by the model concrete due to its thermal mass and resistance, and thus not all of the heat energy was transported to the pile surface. Indeed, at the pile surface, the increase in temperature was 6 – 8 °C in both tests. For Test 3 when pile heating was maintained during the shearing stage (i.e., operational mode), the pile surface temperature continued to rise by a small amount until an increase in surface temperature of almost 10 °C was observed by the end of the test (Fig. 10(a)). These measurements were input in all the exterior surfaces of the three piles in the finite element mesh shown

in Fig. 9. On the contrary, for Test 4, pile heating was stopped after a similar increase in pile surface temperature was achieved as in Test 3 (i.e., shutdown mode) before the shearing stage (Fig. 10(b)); Before shearing started, the pile surface temperature had reduced by almost 5 °C and dropped to a level close to or lower than that in the surrounding soil.



(a)



(b)

Figure 10. Temperature-time histories at the pile surface and the soil in (a) Test 3; and (b) Test 4.

As the pile heat was dissipated to the surrounding soil, the soil temperature at both 1D and 2D away from the pile centre in both tests was increased (Figs 10 and 11). However, the amount of temperature rise in the soil (up to 5 °C) was less significant than that in the pile, primarily because the silt had a lower thermal conductivity and higher heat compacity. It can be seen from

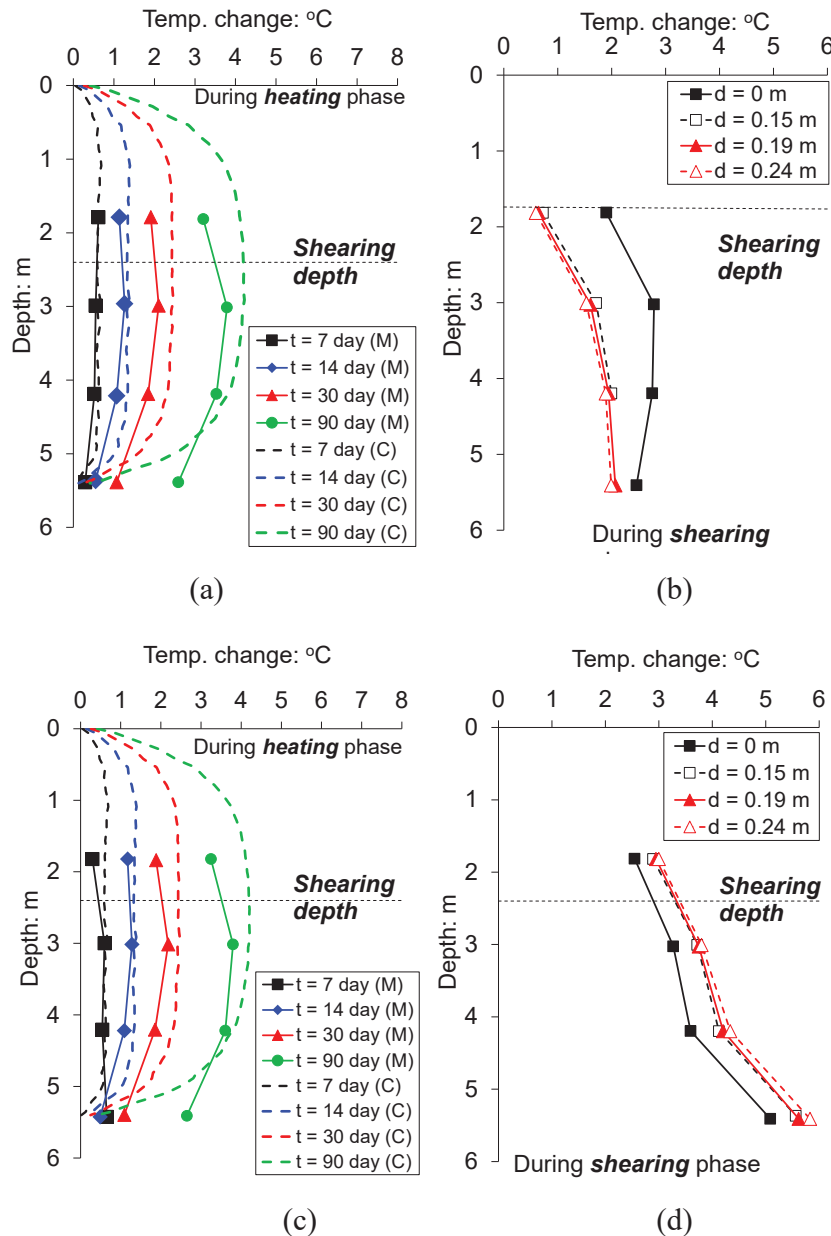


Figure 11. Vertical profiles of soil temperature 1D away from the pile surface at different elapsed time during the heating phase in (a) Test 3 and (c) Test 4, and at different shear displacements (d) during the shearing phase in (b) Test 3 and (d) Test 4. 'M' and 'C' in the legend mean measured and computed results, respectively. Note that the computed results apply to both Tests 3 and 4.

Fig. 11 that as the heating phase progressed in both tests, the soil temperature profile at $1D$ away from the pile centre became more parabolic in shape. This profile shape was consistently found in the FE simulation. The computed contours of soil temperature at sections A-A and B-B are given in Fig. 12. The soil near the top and bottom of the block was cooler than that in between. This was because of evaporation of near surface moisture, which was a cooling process that counteracted the pile heating effect, as well as heat exchange with the atmosphere. The heat transfer from the pile to the surrounding soil was less effective near the pile toe due to (i) the end-effect where the two U-shaped tubes curved away from the pile surface and the cover depth was hence greater and (ii) heat transfer to the aluminium base plate of the LDSA and eventually the thermal mass of the model container of the centrifuge. This heat exchange at the bottom boundary was captured by the FE analysis. The temperature contour shows that there was thermal interaction between the neighbouring piles (spaced $4D$ centre-to-centre) as indicated by the overlapping of the influence zone of temperature. As the shutdown operation mode was activated and the heat supply to the piles was stopped in Test 4 (Figs 10 and 11), there was associated reduction of soil temperature but the magnitude of temperature drop was less significant than that in the piles because of thermal inertia within the silt.

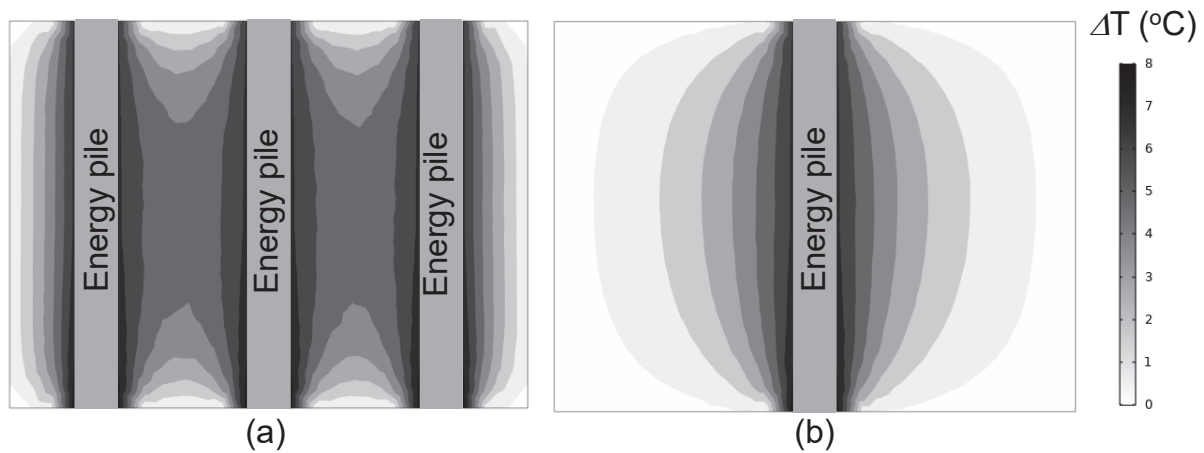
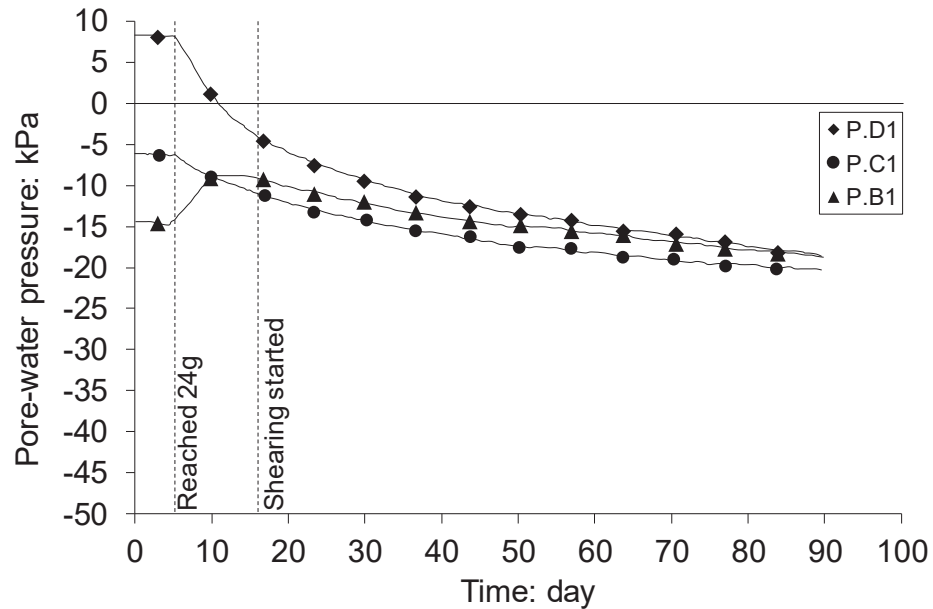


Figure 12. Computed temperature contours of Test 3: (a) Section A-A; (b) Section B-B.

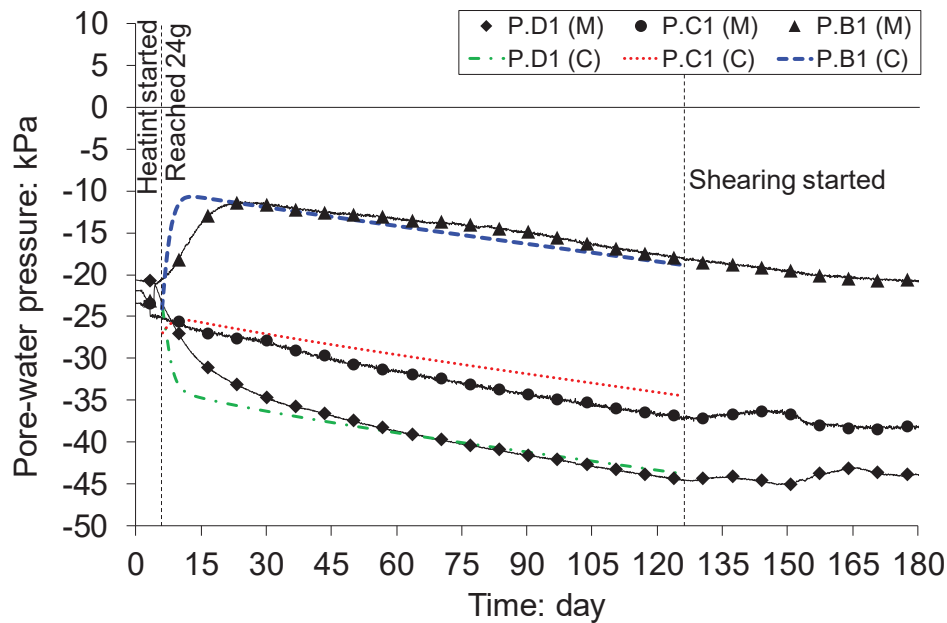
Pore water pressure field

Figures 13(a) and 14(a) show the measured time histories and vertical distribution of PWP measured at $1D$ away from the pile centre for Test 2 using the conventional piles. When 24 g was reached and maintained, there was a consistent reduction of PWP because of the dissipation of the

excess PWP during the rising- g level stage and gravity-driven downward water flow. Before shearing, the PWP ranged between -5 to -10 kPa. During shearing, there were continuous reductions of PWP by approximately 10 kPa and the PWP appeared to converge to an approximately constant value of -19 kPa.



(a)



(b)

Figure 13. Pore water pressure-time histories at $1D$ from the pile surface; (a) Test 2; (b) Test 3.

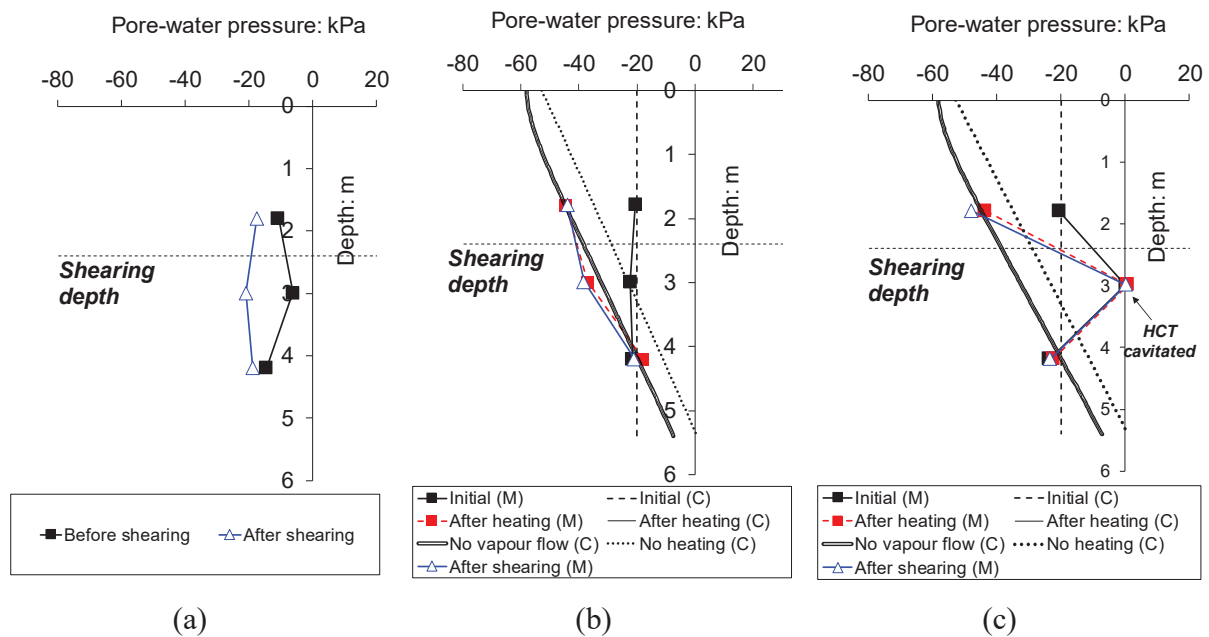


Figure 14. Vertical profiles of pore water pressure (at $1D$ away from the pile surface) obtained during the heating and shearing phases for (a) Test 2; (b) Test 3; and (c) Test 4. Note: M and C in the bracket stands for measured and computed, respectively. In Figs (b) and (c), the computed lines for ‘After heating’ and ‘No vapour flow’ overlap.

The PWP responses, with time and with depth, of Test 3 using energy piles are depicted in Figs 13(b) and 14(b), respectively. During the first five days of pile heating, there was a substantial decrease in PWP at shallower soil depth (i.e. P.D1) with time and yet a further increase in PWP at deeper depth (i.e. P.B1), consistently found from both the measurements and simulations. This was because the initial PWP distribution was uniform with a value of -20 kPa; due to gravity, water at shallow depths (where the total head was relatively high) seeped downward. After the water redistribution during these five days, the PWP at all depths subsequently reduced with time, apparently following the same rate. The measured and computed PWP profiles after heating depicted in Fig. 14(b) both showed that the PWP distributed hydrostatically with a gradient close to the unit weight of water (i.e. 10 kN/m^3). The computed PWP profiles for the two hypothetical cases, (i) without pile heating and (ii) without vapour flow (but with pile heating), are superimposed in the figure. In both cases, similar hydrostatic PWP distribution was found but the magnitude of PWP in case (i) was higher (i.e. less negative) whereas that in case (ii) showed no practical difference. The comparisons highlight that the primary effect of pile heating in Test 3 was an increase in soil

hydraulic conductivity due to the heat-induced reduction of water viscosity (via the term $K_{LT}(T, \psi)$ in Eq. (2)). The gravity-induced downward water flow was thus accelerated by the pile heating. The effects of vapour transport and water-vapour exchange appeared to have only marginal influences on the observed PWP changes. A similar phenomenon was identified in Test 4 (Fig. 14(c)).

Figures 15(a) and (b) show the computed PWP contours for Test 3 after pile heating, while Figures 15(c) and (d) depict the changes of horizontal PWP profiles due to pile heating across the shearing plane at 2.4 m depth. There was an evident drop of PWP near the pile surface as discussed earlier. Due to the thermal interaction between the piles (spaced $4D$ centre-to-centre; section A-A), the PWP between the two piles (e.g. $2D$ away from the pile centre) was lower than that also at $2D$ away from the pile centre at section B-B. Since the effects of vapour transport and vapour-water exchange were minimal in this system, vapour condensation, and hence any associated increase in PWP (like those identified by Baser et al. 2018), in the far field was negligible.

Lateral response of energy pile rows

Figure 16 shows the shear load-displacement curves obtained from all centrifuge tests. The curve obtained from the conventional small-size direct shear apparatus is also shown for comparison, after applying the appropriate scaling laws. The total vertical stress applied in this test was the same as that expected along the sliding plane of the LDSA. While there was a similar initial stiffness between the two unreinforced cases, the silt tested in the LDSA displayed a distinct peak followed by a more prominent post-peak softening response. These differences were attributed to the silt tested in the LDSA being drier (due to water redistribution during centrifuge spin-up) than that in the small shear apparatus, resulting in a higher suction and peak strength. When the silt was reinforced by the conventional pile row (Test 2), the system response was noticeably stiffer and stronger than both the unreinforced cases. The ultimate load at large displacement was 15% to 35% higher. When the energy RC pile row was used and was operational during shearing (Test 3), the pile heating reduced both the initial stiffness and the peak shear load considerably compared to Test 2. Yet the ultimate load (at large displacement) appeared to converge to the same value as that obtained from the conventional RC pile case and the soil-energy pile system was more ductile (i.e., the difference between the peak and residual load were reduced). When the energy RC pile row had been shut-down before shearing (Test 4), the initial stiffness of the soil-energy pile system was similar to that observed in Test 3, yet the peak load was higher. The ultimate load, similarly,

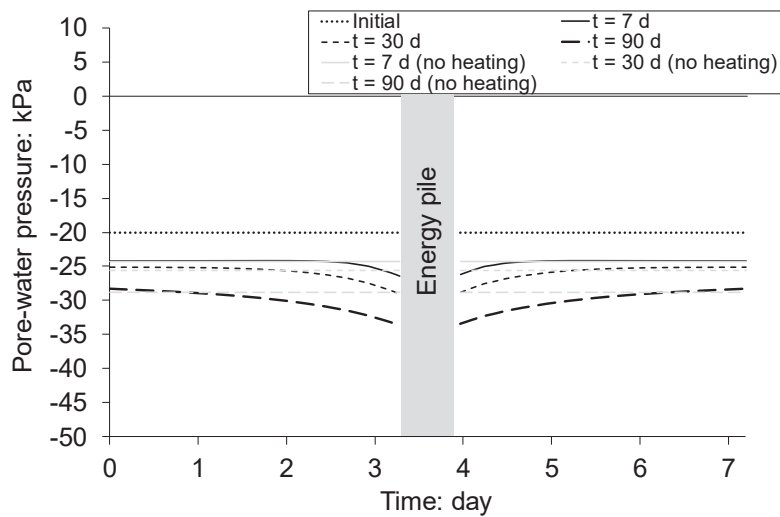
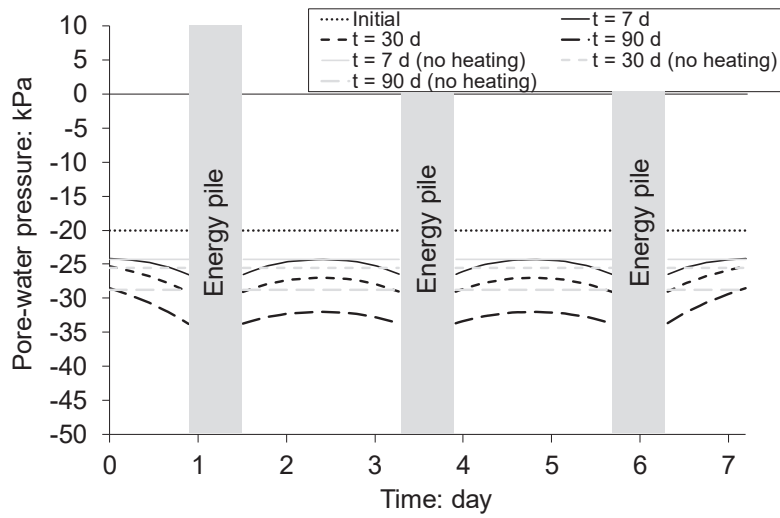
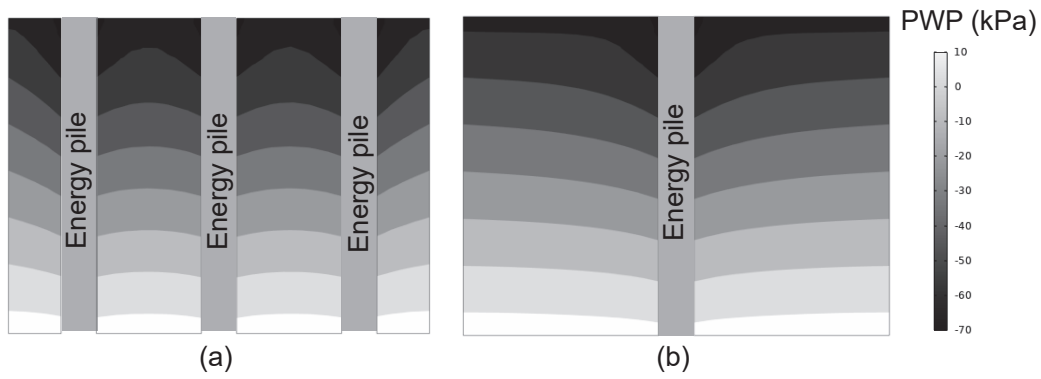


Figure 15. Computed PWP contour of Test 3: (a) Section A-A; (b) Section B-B and computed horizontal PWP distribution at the shearing depth of 2.4 m (c) Section A-A; (d) Section B-B

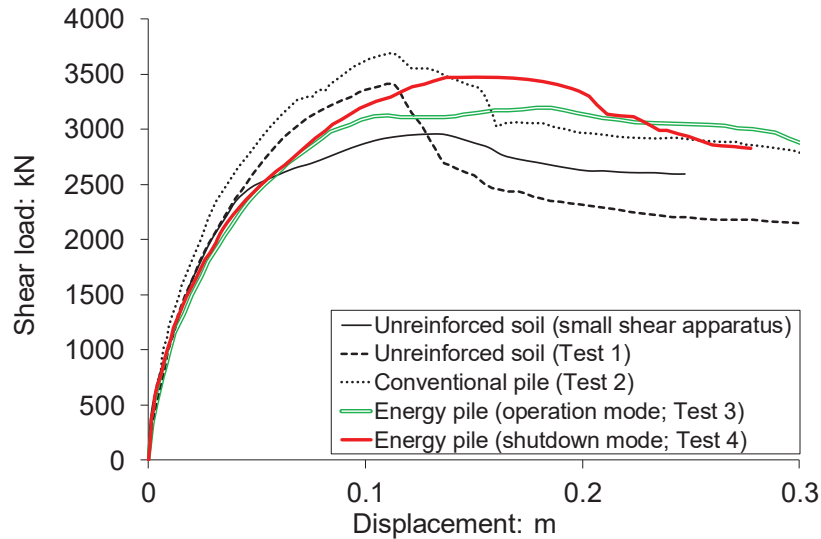


Figure 16. Measured shear load-displacement curves for the unsaturated silt with and without reinforcing by a discrete row of three conventional piles and energy piles

As the silt was heated by the energy pile row, there were two major mechanisms that would be expected to have occurred yet counteract each other. The first one was potential increases in the peak shear strength and stiffness of the unsaturated silt due to the heat-induced increase in matric suction (see Fig. 14). The second mechanism is related to thermal softening, a thermomechanical phenomenon that describes the retraction of yield loci of the soil due to temperature increase. Uchaipichat & Khalili (2009) who conducted triaxial suction- and temperature-controlled drained compression tests showed that the peak deviatoric stress of their compacted silt (similar to the one tested in the present study) reduced when the shearing took place at elevated temperatures. The temperature-induced reduction of peak deviator stress was greater when the initial suction of the silt was higher. At large strain, the deviator stress-strain curves obtained from different temperatures converged to the same single curve, regardless of the confining pressure and matric suction considered. Between these two mechanisms, the centrifuge observed shear behaviour of the soil-energy pile system in Fig. 15 appears to tend to follow the second mechanism.

The implications of these observations are that an energy pile row will act like a conventional reinforcement scheme when the heat transfer systems are inactive. During or shortly after use, there may be greater deformations observed in the slope if the external stressors take it close to

failure. However, if these are sufficient to cause the soil mass to slip, the reinforcement will prevent a sudden brittle failure (sudden large slip) and provide similar resistance to slip as a conventional pile stabilisation scheme (without the thermal functionality) in the post-failure regime.

Figure 16 shows the bending moment profiles of the central model piles instrumented in Tests 2, 3 and 4, showing snapshots at different levels of shear displacement. Note that the pile head was allowed to move freely, so moment at the pile head was set to zero. Positive bending moments correspond to tension on the back side of the pile. When the shearing took place at 2.4 m depth and reached 0.15 m displacement in the case of conventional pile (Test 2), significant moments were mobilised at the back of the bottom part of the pile in the stable soil (i.e., in the soil mass below the shearing plane), whereas much smaller moments were induced in the unstable soil above the plane. When shearing to 0.19 m, the peak moments found in the stable soil grew significantly, yet little further growth was observed in reaching 0.24 m displacement. During the entire shearing process, the moment measured near the shearing plane was close to zero, which is expected because the shear force there was maximum due to the applied lateral pressure from the moving soil. Two peak bending moments may be identified in Test 2, one smaller one in the slipping soil and another larger one in the stable soil. In particular, the bottom-most peak moment was

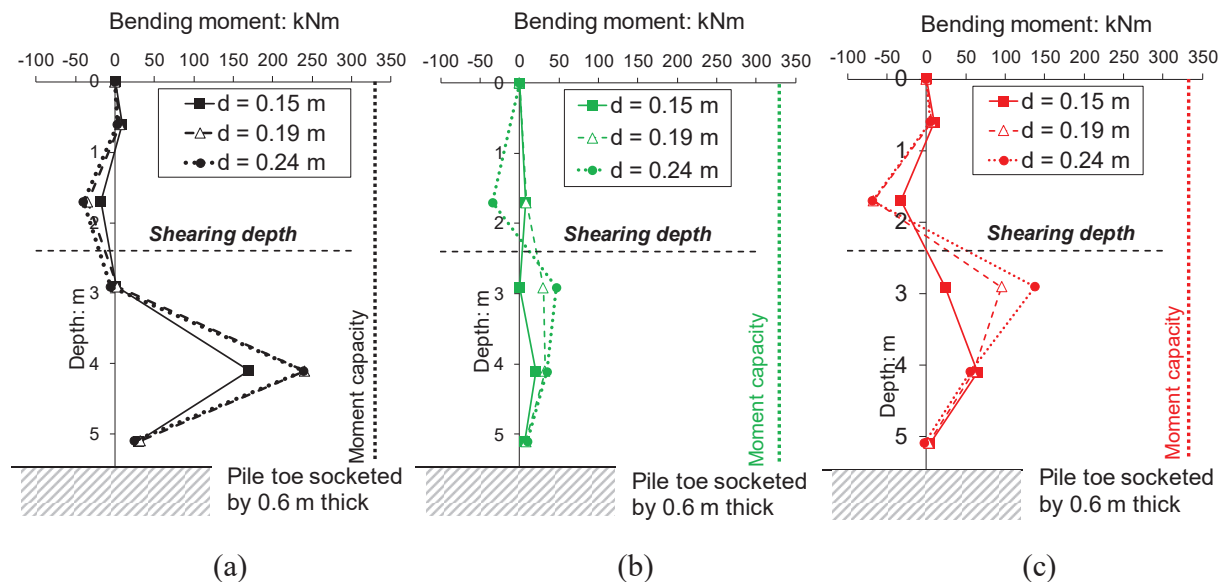


Figure 17. Mobilised bending moment profiles at different shear displacements (d) of 0.15, 0.19 and 0.24 m for the case of (a) conventional pile (Test 2); (b) energy pile in operation mode (Test 3); (c) energy pile in shutdown mode (Test 4). Moment capacity of 336 kNm was determined by the four-point bending tests from Zhao *et al.* (2020).

close to the characteristic structural capacity of the model RC pile (Zhao *et al.*, 2020). Indeed, clear tension cracks were identified at the similar depth of the exhumed pile. Based on the shape of the moment profiles, “soil flow” might have taken place, as suggested by Poulos (1995). In this failure mode, the soil mass above the shearing plane might flow around the upper portion of the piles, fully mobilising the soil strength in the stable mass before the pile flexural strength in the stable strata below the plane can be exceeded (Viggiani, 1981; Kanagasabai *et al.*, 2011).

Similar bending moment profiles were identified from the energy piles tested in Tests 3 and 4, implying that “soil flow mode” might have also occurred in these cases. Yet, the magnitude of the peak bending moments in the stable strata was much smaller than that mobilised in the conventional pile tested in Test 2. Correspondingly, no prominent tension cracks were observed in both the central model piles tested. The depth below the shear plane at which the moment peaked appeared to be shifted to a higher elevation. These observed changes suggested stress redistribution between the soil and the energy piles due to the changes in soil behaviour upon pile heating. The reduced loading on the energy piles at similar soil deformations is consistent with the overall lower stiffness of the combined soil-pile system observed in Fig. 16. According to theoretical analyses of soil plastic flow proposed by Ito & Matsui (1975) and Poulos (1995), at a given pile spacing, piles would attract less lateral force and less bending moment when the surrounding soil is weaker, in this case, because of thermal softening by the pile heating. Although horizontal load may be induced in the pile due to its thermal expansion under lateral restraint by the soil, such an increase is deemed to be negligible due to the relatively small coefficient of thermal expansion of the model RC pile ($15.8 \mu\epsilon/^\circ\text{C}$) and hence small thermal strain (compared to the soil strain during shearing).

These observations suggest that use of a stabilising RC pile row for additional energy transfer functionality will not attract additional flexural stress to the piles during soil displacement and therefore will not adversely affect the structural integrity of the piles under in-service conditions. However, caution should be exercised in case of excessive slope movement (i.e. the piles being loaded to the ultimate limit state), which might introduce tension cracks to the RC pile section and result in potential leakage of the heat-circulating fluid from the embedded pipes, affecting the heat exchange functionality and the subsequent serviceability of the damaged system.

CONCLUDING REMARKS

This study has evaluated the concept of using a discretely spaced energy RC pile row in slope stabilisation schemes to increase soil matric suction, reduce excessive temperatures on bituminous roadways in summer and provide a de-icing solution as an alternative to gritting in winter. The key focus has been on identifying how such use would affect the primary geomechanical stabilisation function of the pile row. To achieve this, centrifuge model tests were conducted to measure the shearing behaviour of unsaturated silt with and without reinforcement by conventional piles and energy piles. Finite element coupled vapour-water-heat transport analysis was performed to further understand the effects of pile heating on the responses of temperature and PWP of the soil.

Continuous heating by three closely-spaced energy piles (i.e. during operation of the energy recovery/storage system in summer or winter) caused reduction of pore water pressure (increases in soil matric suction), particularly near to the soil surface, because of enhanced gravity-driven water flow as a result of an increase in soil hydraulic conductivity when the water viscosity reduced due to pile heating. Although the heat-induced increase in suction might have potentially increased the shear strength of soil in the vicinity of the energy piles, unexpectedly this mechanism did not lead to any increase in the maximum shear capacity of the soil-energy pile system. Indeed, peak reinforcement provided by the energy piles was lower than that observed by the conventional piles. However, at large shear displacements, the additional resistance provided by the energy piles was similar to that provided by the conventional piles yet significantly above the strength of the unreinforced soil. The shearing response of the energy pile row was more ductile than the conventional pile case. The exact underlying mechanism behind this unexpected behaviour is unclear at this stage, but based on existing limited knowledge of the thermo-hydro-mechanical behaviour of unsaturated soil, it is reasonable to hypothesise that the observed reduction of shear capacity due to the pile heating was associated with soil thermal softening, with this mechanism having overwhelmed any beneficial effects associated with suction-induced increase in shear strength. Shearing the pile-reinforced unsaturated soil mobilised pile bending moment. For the given soil type and model RC pile design considered in this study, pile heating reduced the amount of pile moment mobilised at all depths, possibly because of the reduction of soil strength upon thermal softening.

The findings of this study suggest that the piles modified with additional energy transfer functionality would prevent soil from a sudden brittle failure and provide similar ultimate resistance to slip as a conventional pile stabilisation scheme (without the thermal functionality) in

the post-failure regime. Use of a stabilising energy pile row will not attract additional flexural stress to the piles due to the thermal operation and therefore will not adversely affect the structural integrity of the piles during soil displacement. This suggests that the concept of using an energy pile row within road embankments to mitigate some of the extreme weather effects associated with climate change (i.e. reduction in road surface temperatures in summer and road de-icing in winter) could be utilised alongside a primary role in mitigating large deformations associated with ground slip, and warrants further study.

ACKNOWLEDGEMENTS

The first author is grateful for PhD funding support provided by the Energy Technology Partnership (ETP), Scottish Road Research Board (SRRB) via Transport Scotland, the EPSRC Doctoral Training Award as well as the Scottish Funding Council (SFC). The second author would like to acknowledge the funding provided by the National Natural Science Foundation of China (NSFC) under the Excellent Youth Scientist Scheme (H. K. & Macau) (project no. 51922112). The work described in this paper was partially support by a grant from the Research Grants Council of the Hong Kong Special Administrative Region, China (Project No. AoE/E-603/18). The fifth author acknowledges the studentship provided by the Chinese Scholarship Council.

REFERENCES

- Al-Defae, A. H., & Knappett, J. A. (2014). Centrifuge modeling of the seismic performance of pile-reinforced slopes. *J. Geotech. Geoenviron. Engng* 140, No. 6, 1–13.
- Baser, T., Dong, Y., Moradi, A. M., Lu, N., Smits, K., Ge, S., Tartakovsky, D., McCartney, J. S. (2018). Role of nonequilibrium water vapor diffusion in thermal energy storage systems in the vadose zone. *J. Geotech. Geoenviron. Engng*, 144(7): 04018038.
- Brennan, A. J., Knappett, J. A., Bertalot, D., Loli, N., Anatasopoulus, I., & Brown, M. J. (2014). Dynamic centrifuge modelling facilities at the University of Dundee and their application to studying seismic case histories. *Proc. 8th Int. Conf. on Physical Modelling in Geotechnics*. Taylor & Francis Group, London, UK, pp. 227–233.
- Cardarelli, F. (2008). *Materials handbook: a concise desktop reference*. Springer Science & Business Media. London, UK.

- Chung, S.-O., & Horton, R. (1987). Soil heat and water flow with a partial surface mulch. *Water Resources Research*, 23, No. 12, 2175–2186.
- Dixon, N., & Spriggs, M. (2007). Quantification of slope displacement rates using acoustic emission monitoring. *Can. Geotech. J.* 44, No. 8, 966–976.
- EN 1992-1-1 (2004). *Eurocode 2: Design of concrete structures: Part 1-1: General rules and rules for buildings*. British Standards Institution.
- Fredlund, D. G., Morgenstern, N. R., & Widger, R. A. (1978). The shear strength of unsaturated soils. *Can. Geotech. J.* 15, No.3, 313–321.
- Girout, R., Blanc, M., Thorel, L., & Fagundes, D. F. (2016). Arching and deformation in a piled embankment: centrifuge tests compared to analytical calculations. *J. Geotech. Geoenviron. Engng* 142, No.12, 04016069.
- Goode, J. III, & McCartney, J. S. (2015). Centrifuge modeling of boundary restraint effects in energy foundations. *J. Geotech. Geoenviron. Engng* 141, No. 8, 04015034.
- Huges, P. N., Glendinning, S., Davies, O., & Mendes, J. (2008). Construction and monitoring of a test embankment for evaluation of the impacts of climate change on UK transport infrastructure. *Proc. 1st Int. Conf. on Transportation Geotechnics*, CRC Press, Nottingham, London, pp. 495–499.
- Iai, S., Tobita, T., & Nakahara, T. (2005). Generalised scaling relations for dynamic centrifuge tests. *Géotechnique* 55, No.5, 355–362.
- Ito, T., & Matsui, T. (1975). Methods to estimate lateral force acting on stabilising piles. *Soils Found.* 18, No. 4, 43–59.
- Jeong, S., Kim, B., Won, J., & Lee, J. (2003). Uncoupled analysis of stabilizing piles in weathered slopes. *Comput. Geotech.* 30, No.8, 671–682.
- Kanagasabai, S., Smerthurst, J. A., & Powrie, W. (2011). Three-dimensional numerical modelling of discrete piles used to stabilise landslides. *Can. Geotech. J.* 48, No.9, 1393–1411.
- Khalili, N., and Khabbaz, M. H. (1998). A unique relationship for χ for the determination of shear strength of unsaturated soils. *Géotechnique* 48, No.5, 681–688.
- Knappett, J. A., Brown, M. J., Shields, L., Al-Defae, A. H., & Loli, M. (2018). Variability of small scale model reinforced concrete and implications for geotechnical centrifuge testing. *Proc. 9th Int. Conf. on Physical Modelling in Geotechnics*, CRC Press, London, UK, pp. 241–246.
- Knappett, J. A., Reid, C., Kinmond S., & O'Reilly, K. (2011). Small-Scale Modeling of Reinforced

- Concrete Structural Elements for Use in a Geotechnical Centrifuge. *J. Struct. Engng* 137, No.11, 1263–1271.
- Kourkoulis, R. (2009). Interplay of mat foundations and piles with a failing slope. Ph.D. thesis, National Technical Univ. of Athens, Greece.
- Kourkoulis, R., Gelagoti, F., Anastasopoulos, I., & Gazetas, G. (2010). Slope stabilizing piles and pile-groups: parametric study and design insights. *J. Geotech. Geoenviron. Engng* 137, No. 7, 663–677.
- Kourkoulis, R., Gelagoti, F., Anastasopoulos, I., & Gazetas, G. (2012). Hybrid method for analysis and design of slope stabilising piles. *J. Geotech. Geoenviron. Engng* 138, No. 1, 1–14.
- Leung, A. K., Feng, S., Vitali, D., Li, M., & Karimzadeh, A. A. (2020). Temperature effects on hydraulic properties of unsaturated sand and their influences on water-vapor-heat transport. *J. Geotech. Geoenviron. Engng* 146, No. 4, 06020003.
- Liu, X. C. (2017). *Centrifuge modelling and analysis of rainfall-induced shallow failure in unsaturated soil slope*. Ph.D thesis, Zhejiang University, China (in Chinese).
- Loveridge, F., & Powrie, W. (2013). Pile heat exchangers: thermal behaviour and interactions. *Proceedings of the Institution of Civil Engineers-Geotechnical Engineering*, 166, No.2, 178–196. DOI: 10.1680/jeng.11.00042
- Minto, A., Leung, A.K., Vitali, D., & Knappett, J.A. (2016). Thermomechanical properties of a new small-scale reinforced concrete thermo-active pile for centrifuge testing. *Proc.10th Int. Conf. on Energy Geotechnics*, CRC Press/Balkema, Kiel, Germany, pp.37–44.
- National Instruments. (2016). *Measuring strain with strain gauge*. < <http://www.ni.com/white-paper/3642/en/>> (May. 25, 2016)
- Ng, C. W. W., Shi, C., Gunawan, A., & Laloui, L. (2014). Centrifuge modelling of thermo-active piles subjected to heating and cooling cycles in clay. *Géotechnique Letters*, No. 4, 310–316.
- Ng, C. W. W., Shi, C., Gunawan, A., Laloui, L., & Liu, H. L. (2015). Centrifuge modelling of heating effects on energy pile performance in saturated sand. *Can. Geotech. J.* 52, No.8, 1045–1057.
- Potts, D. M., Dounias, G. T., & Vaughan, P. R. (1987). Finite element analysis of the direct shear box test. *Géotechnique* 37, No. 1, 11–23.
- Poulos, H. G. (1995). Design of reinforcing piles to increase slope stability. *Can. Geotech. J.* 32, No.5, 808–818.

- Sassa, K., & Canuti, P. (2009). *Landslides – Disaster risk reduction*. Springer Science & Business Media, Berlin.
- Smethurst, J. A., & Powrie, W. (2007). Monitoring and analysis of the bending behaviour of discrete piles used to stabilise a railway embankment. *Géotechnique* 57, No.8, 663–677.
- Stewart, M. A., & McCartney, J. S. (2014). Centrifuge modeling of soil-structure interaction in energy foundations. *J. Geotech. Geoenviron. Engng* 140, No.4, 04013044.
- Taylor, R. N. (1995). *Geotechnical Centrifuge Technology*. CRC Press, London.
- Toll, D. G., Lourenco, S. D. N., & Mendes, J. (2013). Advances in suction measurements using high suction tensiometers. *Engineering geology*, 165: 29–37.
- Uchaipichat, A., & Khalili, N. (2009). Experimental investigation of thermo-hydro-mechanical behaviour of an unsaturated silt. *Géotechnique* 59, No.4, 339–353.
- van Genuchten, M.T. (1980). A closed-form equation for predicting the hydraulic conductivity of unsaturated soils 1. *Soil Sci. Soc. Am. J.* 44, No.5, 892-898.
- Viggiani, C. (1981). Ultimate lateral load on piles used to stabilize landslides. *Proc. 10th Int. Conf. on Soil Mechanics and Foundation Engineering*, Stockholm, Sweden, vol. 3, pp. 555–560.
- Vitali, D., Leung, A.K., Minto, A., & Knappett, J.A. (2016). A new model reinforced concrete for modelling energy geo-structures in geotechnical centrifuge. In *Geo-Chicago 2016: Sustainability, Energy and Geoenvironment*. Chicago, US, 185–194.
- Vitali, D., Leung, A. K., Zhao, R., & Knappett, J. A. (2018). A new heating-cooling system for centrifuge testing of thermo-active geo-structures. *Proc. 9th Int. Conf. on Physical Modelling in Geotechnics*, London, United Kingdom, vol. 1, pp. 475–480.
- Wilson, G., Fredlund, D. G., & Barbour, S. L. (1997). The effect of soil suction on evaporative fluxes from soil surfaces. *Can. Geotech. J.*, 34, 145–155.
- Wu, D., Liu, H.L., Kong, G. & Li, C. (2019). Thermo-mechanical behavior of energy pile under different climatic conditions. *Acta Geotechnica*, 14, No.5, 1495-1508.
- Wu, P.-K., Matsushima, K., & Tatsuoka, F. (2008). Effects of specimen size and some other factors on the strength and deformation of granular soil in direct shear tests. *Geotech. Test. J.* 31, No.1, 45–64.
- Zhao, R., Leung, A. K., Vitali, D., Knappett, J. A., & Zhou, Z. (2020). Small-scale modelling of thermomechanical behaviour of reinforced concrete energy piles in soil. *J. Geotech. Geoenviron. Engng* 146, No.4, 04020011.

1
2
3
4
5
6
7
8
9
10
11
12
13
14
15
16
17
18
19
20
21
22
23
24
25
26
27
28
29
30
31
32
33
34
35
36
37
38
39
40
41
42
43
44
45
46
47
48
49
50
51
52
53
54
55
56
57
58
59
60
61
62
63
64
65

711 Zhou R. Z. B., Take, W. A., & Ng, C. W. W. (2006). A case study in tensiometer interpretation:
712 centrifuge modelling of unsaturated slope behaviour. *Proc. 4th Int. Conf. on Unsaturated*
713 *Soils*, Carefree, AZ, pp.2300–2311.

Notations

a	A fitting parameter of the van Genuchten (1980)'s equation
c'	Cohesion
$C_s(\theta)$	Volumetric heat capacities of soil
C_L	Volumetric heat capacities of liquid water
C_V	Volumetric heat capacities of water vapour
γ_w	Unit weight of liquid water
h	Heat exchange coefficient
H_r	Relative humidity
$K_L(T, \psi)$	Hydraulic conductivity of liquid water with respect to ψ change
$K_V(T, \psi)$	Hydraulic conductivity of the water vapor with respect to ψ change
$K_{LT}(T, \psi)$	Hydraulic conductivity of liquid water with respect to T change
$K_{VT}(T, \varphi)$	Hydraulic conductivity of water vapor with respect to T change
L_0	Latent heat of vaporisation of liquid water
$\lambda(\theta)$	Moisture-dependent thermal conductivity function
M	Molecular weight of water
m	A fitting parameter of the van Genuchten (1980)'s equation
n	A fitting parameter of the van Genuchten (1980)'s equation
ϕ'	Friction angle
q_L	Fluxes of liquid water
q_V	Fluxes vapor
Q_h	Heat flux
θ_s	Saturated volumetric water content
θ_r	Residual volumetric water content
$\theta(T, \psi)$	Volumetric liquid water content
$\theta_V(T, \psi)$	Volumetric water vapor content
R	Universal gas constant
ρ_w	Water density
S	Matric suction
s_e	Air-entry value
σ	Total normal stress
T	Soil temperature
T_a	Ambient temperature
u_a	Pore air pressure
u_w	Pore water pressure
χ	Effective stress parameter
ψ	Matric suction